Magnesium Technology 2011
Edited by: Wim H. Sillekens, Sean R. Agnew, Neale R. Neelameggham, and Suveen N. Mathaudhu
TMS (The Minerals, Metals & Materials Society), 2011

Magnesium Technology 2011

Deformation Mechanisms I

Session Chairs:

Carlos H. Caceres
(University of Queensland, Australia)
Eric A. Nyberg
(Pacific Northwest National Laboratory, USA)

Magnesium Technology 2011
Edited by: Wim H. Sillekens, Sean R. Agnew, Neale R. Neelameggham, and Suveen N. Mathaudhu
TMS (The Minerals, Metals & Materials Society), 2011

CRYSTAL PLASTICITY ANALYSIS ON COMPRESSIVE LOADING OF MAGNESIUM WITH SUPPRESSION OF TWINNING

Tsuyoshi Mayama[1], Tetsuya Ohashi[2], Kenji Higashida[3], Yoshihito Kawamura[1]
[1]Kumamoto University, 2-39-1, Kurokami, Kumamoto, 860-8555, JAPAN
[2]Kitami Institute of Technology, 165 Koen-cho, Kitami, Hokkaido, 090-8507, JAPAN
[3]Kyushu University, 744 Motooka, Fukuoka, 819-0395, JAPAN

Keywords: Finite element analysis, Crystal plasticity, Compressive loading, Heterogeneous deformation, Twinning

Abstract

The compressive loading behavior of single crystals and bicrystals of magnesium without consideration of deformation twinning has been investigated by crystal plasticity finite element analysis with the aim of fundamental understanding of kink band formation in magnesium alloys with long period stacking ordered structure (LPSO) phase. The basal plane of the single crystal model is set to be parallel to the compressive direction. The result of the compressive loading analysis of single crystals indicates the significant influence of suppression of twinning on the activation of nonbasal slip systems and stress-strain behavior. The compressive analysis of symmetric bicrystal is also performed to clarify the influence of the angle between basal plane and the loading axis. The influence of the introduction of grain boundary and the slight change of crystal orientation is discussed in terms of activated deformation modes.

Introduction

Magnesium alloys with long period stacking ordered (LPSO) structure have attracted great attention. The wrought magnesium alloys with LPSO phase show the excellent mechanical properties [1-3]. It is considered that one of the strengthening mechanisms of these alloys is the formation of kink bands in the LPSO phase. However, the kink band formation mechanism and the influence on the subsequent deformation have not been clarified in detail. Therefore, fundamental research on kink band formation in magnesium is required to gain insight into the strengthening mechanism of magnesium alloys. Fig. 1 shows a TEM image of typical kink bands observed in extruded magnesium alloy $Mg_{96}Zn_2Y_2$.

The previous research on FCC crystals by using crystal plasticity finite element analysis indicates that kink bands perpendicular to the primary slip direction are formed in compatible bicrystals with tilted angle grain boundary under tensile loading [4]. By using the similar numerical method, this study investigates compressive behavior in HCP crystal with suppression of twinning.

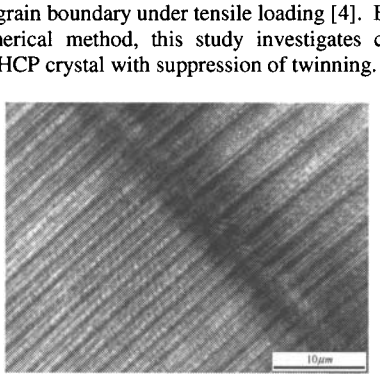

Figure 1. TEM image of kink band in extruded $Mg_{96}Zn_2Y_2$

Crystal plasticity finite element method

A crystal plasticity finite element code developed for face centered cubic (FCC) metals [5, 6] is modified for magnesium. In this study, the words "slip system" and "twin system" are used to indicate the equivalent slip/twin system (slip/twin system family), collectively. The word "deformation mode" is used to indicate the specific one out of equivalent slip/twin system.

Constitutive equations

The critical resolved shear stress $\theta^{(n)}$ on deformation mode n is given by the Schmid law as

$$\theta^{(n)} = \mathbf{P}^{(n)} : \boldsymbol{\sigma} \tag{1}$$

where $\boldsymbol{\sigma}$ denotes the stress tensor. $\mathbf{P}^{(n)}$ is the Schmid tensor of deformation mode n defined by

$$\mathbf{P}^{(n)} = \frac{1}{2}\left(\mathbf{v}^{(n)} \otimes \mathbf{b}^{(n)} + \mathbf{b}^{(n)} \otimes \mathbf{v}^{(n)}\right) \tag{2}$$

where $\mathbf{v}^{(n)}$ and $\mathbf{b}^{(n)}$ are the slip/twin plane normal and the slip/twin direction, vector respectively. The increment of the critical resolved shear stress is written as the following equation:

$$\dot{\theta}^{(n)} = \sum h^{(nm)} \dot{\gamma}^{(m)} \tag{3}$$

where $h^{(nm)}$ and $\dot{\gamma}^{(m)}$ indicate the strain hardening coefficient and the plastic shear strain rate on deformation mode m.

Assuming that the deformation is small and lattice rotation is ignored, the constitutive equation for slip and twin deformation is given by

$$\dot{\varepsilon} = \mathbf{S}^{e} : \dot{\boldsymbol{\sigma}} + \sum\sum \left\{h^{(nm)}\right\}^{-1} \mathbf{P}^{(n)} : \left(\mathbf{P}^{(m)} : \dot{\boldsymbol{\sigma}}\right) \tag{4}$$

where $\mathbf{S}^{e}$ denotes the elastic compliance, and the summation is made over the active deformation modes. We solve the deformation with a rate-independent plasticity formulation.

The following Bailey-Hirsch type model of the critical resolved shear stress is used,

$$\theta^{(n)} = \theta_0 + \sum \Omega^{(nm)} a \mu \tilde{b}^{(n)} \sqrt{\rho_s^{(m)}} \tag{5}$$

where θ_0, a, μ, $\tilde{b}^{(n)}$ and $\rho_s^{(m)}$ denote the lattice friction term, a numerical factor on the order of 0.1, the elastic shear modulus, the magnitude of the Burgers vector for **<a>** dislocation and the statistically stored dislocation (SSD) density that accumulates on deformation mode m, respectively. Although Burgers vector for **<a>** dislocation and **<a+c>** dislocation are different, in this study, for simplicity, the magnitude of Burgers vector of **<a>** dislocation is used in Eq.(5) for all slip/twin systems. By substituting the

derivation of Eq.(5) into Eq.(3), the strain hardening coefficient $h^{(nm)}$ in Eq.(3) is specified. The increment in the SSD density on deformation mode n is given as follows:

$$\rho_S^{(n)} = \frac{c\dot{\gamma}^{(n)}}{\tilde{b}^{(n)} L^{(n)}} \tag{6}$$

Here, $\tilde{b}^{(n)}$ is the magnitude of Burgers vector for deformation mode n. For magnesium, the magnitude of Burgers vector $\tilde{b}^{(a)}$ is used for slip system with slip direction **<a>** and the magnitude of Burgers vector $\tilde{b}^{(a+c)}$ is used for slip system with slip direction **<a+c>**. Burgers vector $\tilde{b}^{(a+c)}$ is calculated by

$$\tilde{b}^{(a+c)} = \tilde{b}^{(a)}\sqrt{1+(c/a)^2} \tag{7}$$

where c/a is axial ratio for HCP crystal structure.
In Eq.(6), c is a numerical coefficient on the order of 1 and $L^{(n)}$ is the mean free path of dislocations on deformation mode n defined as

$$L^{(n)} = \frac{c^*}{\sqrt{\sum_m \omega^{(nm)}\left(\rho_S^{(m)} + \left\|\rho_G^{(m)}\right\|\right)}} \tag{8}$$

where c^* and $\omega^{(nm)}$ are a material constant of the order of 10-100 and the weight matrix, respectively. $\left\|\rho_G^{(m)}\right\|$ denotes the norm of geometrically necessary dislocation (GND) density on deformation mode m defined as

$$\left\|\rho_G^{(m)}\right\| = \sqrt{\left(\rho_{G,edge}^{(m)}\right)^2 + \left(\rho_{G,screw}^{(m)}\right)^2} \tag{9}$$

where the edge and screw components are defined by the strain gradient:

$$\rho_{G,edge}^{(m)} = -\frac{1}{\tilde{b}^{(m)}}\frac{\partial \gamma^{(m)}}{\partial \xi} \quad , \quad \rho_{G,screw}^{(m)} = \frac{1}{\tilde{b}^{(m)}}\frac{\partial \gamma^{(m)}}{\partial \zeta}. \tag{10}$$

Here, ξ and ζ denote directions parallel and perpendicular to the slip direction, respectively.

Slip systems

Because of the lower symmetry in materials with an HCP structure compared to materials with a cubic crystal structure, slip systems for magnesium are classified into different slip system families. The operative slip systems in magnesium have been previously investigated [7-11]. Basal slip system $(0001)\langle 11\bar{2}0\rangle$, prismatic slip system $\{10\bar{1}0\}\langle 11\bar{2}0\rangle$ and first order pyramidal (pyramidal-1) slip system $\{10\bar{1}1\}\langle 11\bar{2}0\rangle$ have long been known. Although Yoshinaga and Horiuchi [12] suggested that magnesium single crystal showed no activation of second order pyramidal (pyramidal-2) slip system $\{11\bar{2}2\}\langle 11\bar{2}3\rangle$, Obara et al. [13] reported the activation of this pyramidal-2 slip system based on slip line analysis and dislocation observation. Recent crystal plasticity studies also incorporate the pyramidal-2 slip system to compensate deformation in the c-axis direction and the results of calculations show quantitatively good agreements with experimental results. Therefore, in the present study, basal, prismatic, pyramidal-1 and pyramidal-2 slip systems in Fig.2 are considered. Table 1 shows the slip plane, the shear direction and the number of deformation modes.

Deformation twinning

Besides slip deformation, another important deformation mechanism for HCP metals is deformation twinning. In magnesium, the contribution of c-axis tensile twinning system $\{10\bar{1}2\}\langle 10\bar{1}1\rangle$ as shown in Fig.1(e) to macroscopic deformation is significantly larger than those by the other twinning systems observed in the experimental studies [12, 14, 15]. Therefore, only the c-axis tensile twinning system is considered in this study because the focus of this study is on the relationships between heterogeneous deformation and activated deformation modes in magnesium. The twin plane, shear direction and the number of deformation mode of twin system $\{10\bar{1}2\}\langle 10\bar{1}1\rangle$ are shown in Table 2. In this study, the twinning deformation is incorporated into crystal plasticity analysis in a similar manner to slip deformation [16]. That is, it is assumed that the twinning plane normal vector and the shear direction vector by twinning are equivalent to the slip plane normal $\mathbf{v}$ and the slip direction vector $\mathbf{b}$, respectively. However, the following two points are considered only for twinning system.

1. In order to simulate the polarity of twinning, shear slip rate is set to be zero when the compressive loading in c-axis.
2. Shear strain by twinning is limited to the maximum value determined by

$$\gamma^{\max} = \frac{\sqrt{3}}{c/a} - \frac{c/a}{\sqrt{3}}. \tag{11}$$

When the accumulated shear strain reaches the maximum value in Eq.(10), the shear strain rate for twinning is set to be zero.

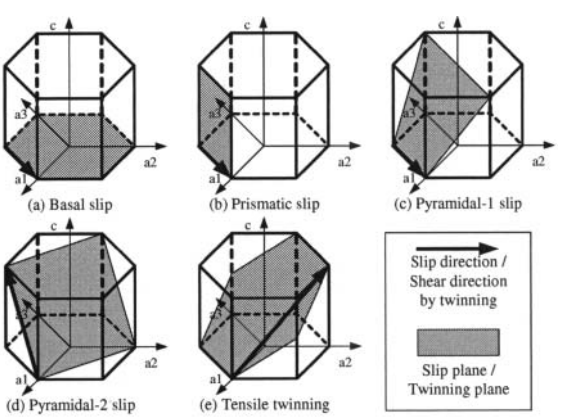

Figure 2. Schematic diagram of slip/twin systems in magnesium

Table 1. Deformation mechanisms in magnesium

Slip/twin system	Slip/twin plane	Shear direction	Number of deformation modes
Basal slip	(0001)	$\langle 11\bar{2}0\rangle$	3
Prismatic slip	$\{10\bar{1}0\}$	$\langle 11\bar{2}0\rangle$	3
Pyramidal-1 slip	$\{10\bar{1}1\}$	$\langle 11\bar{2}0\rangle$	6
Pyramidal-2 slip	$\{11\bar{2}2\}$	$\langle 11\bar{2}3\rangle$	6
Tensile twinning	$\{10\bar{1}2\}$	$\langle 10\bar{1}1\rangle$	6

Anisotropic elasticity for HCP crystal

The anisotropy of elastic deformation of HCP single crystal is taken into account in the present method. The elastic compliances used in this study are shown in Eq. (12).

$$\begin{pmatrix} s_{11} & s_{12} & s_{13} & 0 & 0 & 0 \\ s_{12} & s_{11} & s_{13} & 0 & 0 & 0 \\ s_{13} & s_{13} & s_{33} & 0 & 0 & 0 \\ 0 & 0 & 0 & 2(s_{11}-s_{12}) & 0 & 0 \\ 0 & 0 & 0 & 0 & s_{55} & 0 \\ 0 & 0 & 0 & 0 & 0 & s_{55} \end{pmatrix} \quad (12)$$

here $2(s_{11}-s_{12})$ and s_{55} show shear components of elastic compliance on basal plane and plane perpendicular to basal plane, respectively.

Material parameters for pure magnesium single crystal

Identification of material parameters used in the constitutive equations is very difficult for magnesium. One of the reasons of this difficulty is that the deformation mechanisms and the critical resolved shear stresses (CRSSs) for magnesium have not yet been fully clarified experimentally. The difference of CRSSs between basal slip and nonbasal slip is so significant that deformations by single slip of nonbasal slip hardly occur. Furthermore, the details of strain hardening behavior for each deformation mode and the interaction between dislocations have not been clarified so far. In this study, CRSSs for basal and nonbasal slip systems are set to be 0.5 and 40 MPa based on the experimental reports for pure magnesium single crystal in the literatures [12, 17-21],. To suppress the activation of twinning, CRSS for tensile twinning system is set to be large enough value. The material parameters a, c, c^* used in this study are typical values from the previous studies for FCC metals [5, 6]. Assuming initially uniform dislocation density, the initial dislocation density 10^9 -/m^2 is used for all deformation modes. For the interaction matrix $\Omega^{(nm)}$ in Eq.(5), $\Omega^{(nm)}=1$ for the diagonal components and $\Omega^{(nm)}=1.01$ for the off-diagonal components are assumed. For the weight matrix $\omega^{(nm)}$ in Eq.(8), $\omega^{(nm)}=0$ when n=m or deformation mode n and deformation mode m are the same slip/twin system family. For all other components $\omega^{(nm)}=1$ is assumed. Lattice friction stresses for each slip/twin system are calculated by Eq.(5) using the CRSSs and initial SSD density. Anisotropic elastic constants [22] and the axial ratio [23] for magnesium are used.

Analysis models

Although the deformation modes for HCP materials are conventionally described by Millar-Bravais system as shown in Fig.3(a), an orthonormal system shown in Fig.3(b) is used for convenience of numerical implementation. In the present definition of orthonormal system, three axes $\mathbf{e}_1$, $\mathbf{e}_2$ and $\mathbf{e}_3$ are corresponding to $[10\bar{1}0]$- , $[\bar{1}2\bar{1}0]$- and [0001]- directions, respectively. This orthonormal system is similar to the one used in Staroselsky and Anand [16] except that they defined three axes $\mathbf{e}_1$, $\mathbf{e}_2$ and $\mathbf{e}_3$ as $[\bar{1}2\bar{1}0]$- , $[\bar{1}010]$- and [0001]- directions, respectively. Crystal orientations for each grain are specified by Euler angles κ, θ and ϕ. In the present definition of Euler angles, first, a crystal lattice whose $[10\bar{1}0]$- , $[\bar{1}2\bar{1}0]$- and [0001]-directions in crystal coordinate system are corresponding to x-, y- and z-directions in sample coordinate system, is rotated by ϕ around [0001]-axis. Then, the lattice is rotated by θ around $[10\bar{1}0]$- axis. Finally, the lattice is rotated by κ around [0001]-axis.

In the literature [24, 25], the HCP material whose basal plane is nearly parallel to the loading direction, deforms with kink band formation during compression. Therefore, in this study, the analysis models shown in Fig. 4 are used to investigate the compressive deformation behavior in HCP crystal with suppression of twinning. The compressive directions of the single crystal models $\langle 11\bar{2}0\rangle$ SC and $\langle 10\bar{1}0\rangle$ SC in Fig. 4(a) and (b) are $\langle 11\bar{2}0\rangle$- and $\langle 10\bar{1}0\rangle$- directions, respectively. Euler angles (κ,θ,ϕ) for $\langle 11\bar{2}0\rangle$ SC and $\langle 10\bar{1}0\rangle$ SC are (60°,0°,0°) and (30°,0°,0°). Fig. 4(c) shows the bicrystal model in which the angle between basal plane and compressive direction is α. In this study, four angles are chosen. Euler angles and angles α for bicrystal models are shown in Table 2.

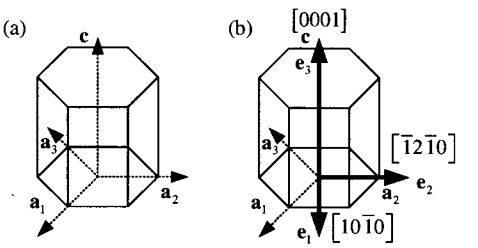

Figure 3. Coordinate system for HCP crystal, (a) Miller-Bravis coordinate, (b) Orthonormal coordinate

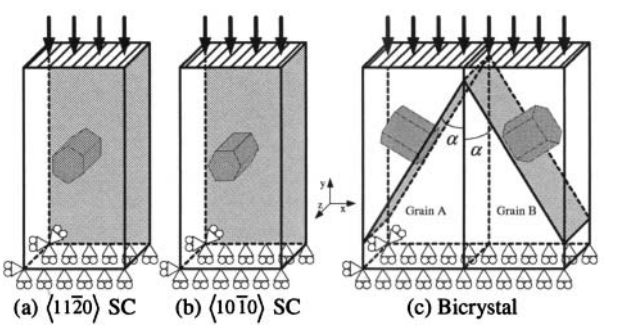

Figure 4. Schematic diagrams of analysis models

Table 2. Euler angles and angle α for bicrystal models

Model name	Euler angles (κ,θ,ϕ)	Angle α
BC5	(330°,270°,85°) for grain A (330°,90°,95°) for grain B	5°
BC15	(330°,270°,75°) for grain A (330°,90°,105°) for grain B	15°
BC30	(330°,270°,60°) for grain A (330°,90°,120°) for grain B	30°
BC44	(330°,270°,46°) for grain A (330°,90°,134°) for grain B	44°

Results and Discussion

Single crystal compression

In Fig. 5, solid lines show the compressive stress-strain curves of $\langle 11\bar{2}0\rangle$ SC and $\langle 10\bar{1}0\rangle$ SC models. The results with consideration of twinning using CRSS of 3MPa for tensile twinning system are also shown in Fig. 5 by broken lines. Depending on the crystal orientation and the consideration of twinning, different stress-strain curves are obtained. Table 3 shows activated deformation

modes during compression. The models without consideration of twinning deform by multiple slip of nonbasal slip system. Activated slip systems in $\langle 11\bar{2}0\rangle$ SC and $\langle 10\bar{1}0\rangle$ SC are pyramidal-2 and prismatic slip system, respectively. This difference in activated slip systems results in the different stress-strain curves shown in Fig. 5. In the case with consideration of twinning, single crystals are deformed by a twinning system. The number of activated twin systems is different in $\langle 11\bar{2}0\rangle$ SC and $\langle 10\bar{1}0\rangle$ SC. Owing to the number of activated twin systems, stress-strain responses are different as shown in Fig. 5. In all cases, the basal slip system is not activated because the Schmid factor for basal slip system is zero. Additionally deformation of these single crystals is almost uniform. These results suggest that any triggers for non-uniform deformation are necessary to activate the basal slip system.

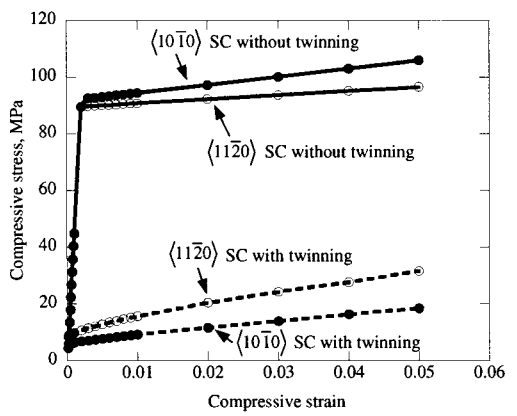

Figure 5. Stress-strain curves in single crystal compression

Table 3. Activated deformation modes in single crystal compression

Model	Activated deformation modes
$\langle 11\bar{2}0\rangle$ SC without twinning	$(11\bar{2}2)[11\bar{2}3]$, $(\bar{1}\bar{1}22)[11\bar{2}3]$
$\langle 10\bar{1}0\rangle$ SC without twinning	$(1\bar{1}00)[11\bar{2}0]$, $(10\bar{1}0)[\bar{1}2\bar{1}0]$
$\langle 11\bar{2}0\rangle$ SC with twinning	$(10\bar{1}2)[\bar{1}011]$, $(01\bar{1}2)[0\bar{1}11]$ $(\bar{1}012)[10\bar{1}1]$, $(0\bar{1}12)[01\bar{1}1]$
$\langle 10\bar{1}0\rangle$ SC with twinning	$(01\bar{1}2)[0\bar{1}11]$, $(0\bar{1}12)[01\bar{1}1]$

Bicrystal compression

Fig. 6 shows the calculated stress-strain curves of compression of bicrystals. With decreasing angle α the flow stress increases. Table 4 shows activated deformation modes in each bicrystal model. In BC5 and BC15 models, nonbasal slip systems are activated as well as the activation of basal slip systems. The increase in the flow stress with decreasing angle α shown in Fig.6 is considered a consequence of more significant hardening by larger accumulated slip of basal slip system with lower Schmid factor. Comparing BC5 with $\langle 11\bar{2}0\rangle$ SC, it is suggested that the introduction of grain boundary and the slight change of crystal orientation result in the activation of basal slip systems. The activation of the basal slip systems probably result in the lower flow stress in BC5 as compared with $\langle 11\bar{2}0\rangle$ SC.

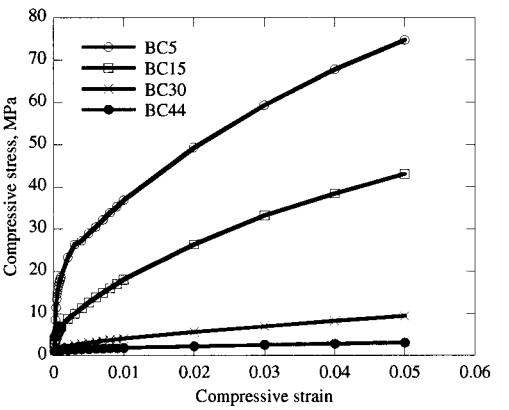

Figure 6. Stress-strain curves in bicrystal compression

Table 4. Activated deformation modes in bicrystal compression

Model	Activated deformation modes
BC5	$(0001)[11\bar{2}0]$, $(0001)[\bar{1}2\bar{1}0]$, $(0001)[\bar{2}110]$ $(10\bar{1}0)[\bar{1}2\bar{1}0]$, $(01\bar{1}0)[\bar{2}110]$, $(\bar{1}\bar{1}22)[11\bar{2}3]$
BC15	$(0001)[11\bar{2}0]$, $(0001)[\bar{1}2\bar{1}0]$, $(0001)[\bar{2}110]$ $(10\bar{1}0)[\bar{1}2\bar{1}0]$, $(01\bar{1}0)[\bar{2}110]$, $(\bar{1}\bar{1}22)[11\bar{2}3]$
BC30	$(0001)[11\bar{2}0]$, $(0001)[\bar{1}2\bar{1}0]$, $(0001)[\bar{2}110]$
BC44	$(0001)[11\bar{2}0]$, $(0001)[\bar{1}2\bar{1}0]$, $(0001)[\bar{2}110]$

Conclusions

In this study, compressive loading behavior of HCP crystal with suppression of twinning was investigated using a crystal plasticity finite element method. From the calculated results of single crystals and bicrystals the following conclusions were obtained.

1. Single crystals compressed in $\langle 11\bar{2}0\rangle$- and $\langle 10\bar{1}0\rangle$-directions deformed uniformly by the multiple slip of nonbasal slip system although the similar analysis with consideration of twinning resulted in the activation of twinning system.
2. In the results of compression analyzes of bicrystal models which had symmetric grain boundaries, the stress-strain behavior and activated deformation modes depended on the angle between basal plane and compressive direction.
3. Comparison between $\langle 11\bar{2}0\rangle$ SC and BC5 suggested that the introduction of grain boundary and the slight change of crystal orientation lead to the activation of basal slip systems. The lower flow stress in BC5 seems to be caused by the basal slip activation.

Comparison of the present results with experimental ones was one of the most interesting points, while there were some difficulties in preparation of LPSO phase single crystals and direct comparison was not made in this paper. Further development of experimental and numerical technique is required in the future research.

Acknowledgements

The work of T.M. was partially supported by a Grant-in-Aid for Scientific Research from the Ministry of Education, Culture, Sports, Science and Technology of Japan (KAKENHI: No.21760082) and the Kumamoto Prefecture Collaboration of Regional Entities for the Advancement of Technological Excellence from Japan Science and Technology Agency.

References

1. Y. Kawamura, K. Hayashi, A. Inoue and T. Masumoto, "Rapidly solidified powder metallurgy $Mg_{97}Zn_1Y_2$ alloys with excellent tensile yield strength above 600MPa" *Materials Transactions* 42 (2001) 1172-1176.
2. S.Yoshimoto, M. Yamasaki and Y. Kawamura, "Microstructure and mechanical properties of extruded Mg-Zn-Y alloys with 14H long period ordered structure" *Materials Transactions* 47 (2006) 959-965.
3. Y.Kawamura and M.Yamasaki, "Formation and mechanical properties of $Mg_{97}Zn_1RE_2$ alloys with long-period stacking ordered structure" *Materials Transactions* 48 (2007) 2986-2992.
4. R.Kondou and T.Ohashi, "Grain boundary accumulation of geometrically necessary dislocations and asymmetric deformations in compatible bicrystals with tilted angle grain boundary under tensile loading" *JSME International Journal A* 49 (2006), 581-588.
5. T.Ohashi, "Three dimensional structures of the geometrically necessary dislocations in matrix-inclusion systems under uniaxial tensile loading" *International Journal of Plasticity* 20 (2004), 1093-1109.
6. T.Ohashi, "Crystal plasticity analysis of dislocation emission from micro voids" *International Journal of Plasticity* 21 (2005), 2071-2088.
7. R.E. Read-Hill and W.D. Robertson, "Deformation of magnesium single crystals by nonbasal slip" *Journal of Metals Transactions of AIME* (1957) 496-502.
8. R.E. Read-Hill and W.D. Robertson, "Pyramidal slip in magnesium" *Transactions of the Metallurgical Society of AIME* 212 (1958) 256-259.
9. W.F. Sheely and R.R. Nash, "Mechanical properties of magnesium monocrystals" Transactions of Metallurgical Society of AIME 218 (1960) 416-423.
10. P. Ward Flynn, J. Mote and J.E. Dorn, "On the thermally activated mechanism of prismatic slip in magnesium single crystals" *Transactions of Metallurgical Society of AIME* 221 (1961) 1148-1154.
11. P.B. Hirsch and J.S. Lally, "The deformation of magnesium single crystals" *Philosophical Magazine* 12 (1965) 595-648.
12. H. Yoshinaga and R. Horiuchi, "Deformation mechanisms in magnesium single crystals compressed in the direction parallel to hexagonal axis" *Transactions of JIM* 4 (1963) 1-8.
13. T. Obara, H. Yoshinaga, S. Morozumi, "{11-22}<-1-123> slip system in magnesium" *Acta Metallurgica* 21 (1973) 845-853.
14. E.W. Kelly and W.F. Hosford, "Plane-strain compression of magnesium and magnesium alloy crystals" *Transactions of Metallurgical Society of AIME* 242 (1968) 5-13.
15. M.R. Barnett, "Twinning and the ductility of magnesium alloys part II. Contraction twins" *Materials Science and Engineering A* 464 (2007) 8-16.
16. A. Staroselsky and L. Anand, "A constitutive model for hcp materials deforming by slip and twinning: Application to magnesium alloy AZ31B" *International Journal of Plasticity* 19 (2003) 1843-1864.
17. E.C. Burke and W.R. Hibbard, "Plastic deformation of magnesium single crystals" Journal of Metals Transactions of AIME (1952) 295-303.
18. H. Yoshinaga and R. Horiuchi, "On the flow stress of alpha solid solution Mg-Li alloy single crystals" Transactions of JIM 4 (1963) 134-141.
19. H. Yoshinaga and R. Horiuchi, "On the nonbasal slip in magnesium crystals" Transactions of JIM 5 (1963) 14-21.
20. A. Akhtar and E. Teghtsoonian, "Solid solution strengthening of magnesium single crystal-I alloying behaviour in basal slip" Acta Metallurgica 17 (1969) 1339-1349.
21. A. Akhtar and E. Teghtsoonian, "Solid solution strengthening of magnesium single crystal-II the effect of solute on the ease of prismatic slip" Acta Metallurgica 17 (1969) 1351-1356.
22. G. Simmons and H. Wang, *Single crystal elastic constants and calculated aggregate properties, second ed.* (The MIT Press, 1971)
23. M.H. Yoo, "Slip, twinning and fracture in hexagonal close-packed metals" *Metallurgical Transactions A* 12 (1981) 409-418.
24. E. Orowan, "A type of plastic deformation new in metals" Nature 149 (1942) 643-644.
25. J.B. Hess and C.S. Barrett, "Structure and nature of kink bands in zinc" Metals Transactions 185 (1949) 599-606.